Supporting Online Material:

Sample Collection: Bulk leaf mats and single leaves were sampled from the Berkeley Museum of Paleontology collection (Fig. DR1). Fossil leaf materials derive from localities at 162 to ~1600 m modern elevation and collected from the same stratigraphic horizon. A range of ages is reported in the literature (49-52 Ma), and recent correlations with invertebrate faunal assemblages place materials in the Capay stage (50.5 to 53 Ma) of invertebrate fauna (Squires, 1997). Leaf assemblages indicate a relatively consistent riparian, angiosperm-dominated forest consisting of 54% trees, 36% shrubs, and 10% vines along the length of the paleochannels. A number of leaf-bearing sample localities overlap authigenic clay sample localities from a previous paleoelevation study of hydrogen isotopes of authigenic kaolinite (Mulch et al., 2006) and of volcanic glasses (Cassel et al., 2009). Sample localities are referenced by the channel distance from the Eocene shoreline, which is marked by the transition to the coastal/marine Ione formation, and along a line (A-A') perpendicular to the modern range. No extractable, leaf-bearing, organic-rich sediments were identified in the region 10-30 km from the Eocene shore.

N-alkane δD as a proxy for $\delta D_{precipitation}$: Long carbon-chain *n*-alkanes are abundantly produced on the surface of leaves, aiding in water repellency and protection from UV radiation or invasive organisms and disease (Holloway, 1969; Barthlott and Neinhuis, 1997), and are commonly preserved in organic sediments without post-depositional isotopic exchange (Schimmelman et al., 1999, Yang and Huang, 2003). Compounds isolated from fossil leaf mats are derived from a variety of plant or microbial sources, but are constrained to angiosperm tree leaves through paleobotanical analyses of leaf materials and the long-chain lengths of compounds examined ($n$$C_{25}$ to $n$$C_{33}$) (Eglington et al., 1967; Cranwell et al., 1987).

To quantify changes in δD with distance from the Eocene shoreline and across the ancient Sierra range, we assume a constant value of -125‰ for $\varepsilon_{apparent}$. Over small spatial scales with high relative humidity, constant vegetation, and single temporal period, this is a reasonable assumption, falling within the range of measured angiosperm fractionation, and leads to estimates of δD_{precip} at the Eocene shoreline that is nearly identical with the value determined by Mulch et al. 2006 from authigenic kaolinites.

Isotopic Analysis of n-Alkanes: The stable hydrogen and carbon isotope composition of *n*-alkanes were measured on a Thermo Trace 2000 GC with Trace GC combustion ($\delta^{13}C$) or High Temperature Conversion system (δD) coupled to a ThermoFinnigan Delta Mat 253. Typical analytical precision for δD analyses of high molecular weight compounds is ±3‰.

Leaf mats are preserved in fine clay layers in Eocene gravels positioned well above modern river channels. Compounds extracted from individual leaves in leaf mats preserve isotopic and compound abundance differences and are D-enriched by at least 20‰ relative to ancient leaf-wax compounds across the range (*B. Tipple Personal Comm.*).

Odd over Even Preference: The CPI is an indication of *n*-alkane source and is defined:

$$CPI = \tfrac{1}{2}\left(\left(nC_{25} + nC_{27} + nC_{29} + nC_{31} + nC_{33}\right)/\left(nC_{24} + nC_{26} + nC_{28} + nC_{30} + nC_{32}\right) + \left(nC_{25} + nC_{27} + nC_{29} + nC_{31} + nC_{33}\right)/\left(nC_{26} + nC_{28} + nC_{30} + nC_{32} + nC_{34}\right)\right)$$

N-alkanes derived from land plants commonly display predominance of odd-numbered carbon chains with CPI > 5, while petrogenic or marine inputs are characterized by considerably lower (CPI ~1). CPI values vary from 2.8 to 5.0, but show no systematic relationship with distance from the Eocene shore or with measured *n*-alkane δD, showing little evidence for post-depositional alteration.

Methylation and Cyclization Indices of Branched Tetraethers: Glycerol dialkyl glycerol tetraethers (GDGT) are membrane lipids produced by anaerobic soil microorganisms (Sinninghe Damsté, et al. 2000; Schouten et al., 2000). The relative amount of methyl branches and the degree of cyclization in GDGT compounds is linearly related to the mean-annual air temperature and pH, respectively (Weijers et al 2007a). The relative degree of methylation is expressed in terms of an MBT (Methyl Branched Tetraethers) index, which specifically represents the degree of methylation at position C-5. The relationship between the number of cyclopentyl rings and pH is quantified by the "CBT" index (Cyclization of Branched Tetraethers)(Weijers et al., 2007a). The relationship between CBT, MBT, pH, and temperature is described by a two-component equation and highlights the strong environmental controls on membrane composition:

$MBT = 0.122 + 0.187*CBT + 0.020*MAT$ ($R^2 = 0.77$)

$CBT = 3.33-0.38*pH$ ($R^2 = 0.70$)

where MAT is the mean annual temperature, and MBT and CBT are defined as:

$MBT = [I + Ib + Ic]/[[I+Ib+Ic]+[II+IIb+IIc]+[III+IIIb+IIIc]]$

$CBT = -\log[(Ib+IIb)/(I+II)]$

Roman numerals indicate abundances of the different GDGT isomers. High MBT values reflect a low degree of methylation and high temperatures and high CBT values reflect low pH (Weijers et al., 2007a).

GDGTs are resistant to degradation by oxidation-reduction reactions or acidic/basic conditions because their strong ether linkages, stable at temperatures below 150°C, and show little change in compound distribution at temperatures up to 240°C (Schouten et al., 2004; Huguet, 2007). While GDGTs are subject to degradation over time (Schouten et al., 2003), there

is little reason to suspect differential diagenesis between compounds (Schouten et al., 2003; Sluijs et al., 2006). Ancient Sierra Nevada sediments have remained within several hundred meters of the modern surface and have thus not been exposed to high burial temperatures.

Samples were analyzed by high performance liquid chromatography/atmospheric pressure chemical ionization mass spectrometry (HPLC/APCI-MS) on an Agilent single quad LC/MS 6100 series at Yale University. Analysis of GDGT compounds at Yale University produces nearly identical results to measurements at the Royal Netherlands Institute for Sea research (NIOZ) and Harvard University (A. Pearson) and are within 1°C for TEX_{86} and MBT/CBT temperatures. Reproducibility of calculated temperatures is within 1.5°C for all analyses.

We analyzed fifteen soils from forests of the modern northern Sierra Nevada to determine the potential for modern contamination of ancient sediments. Modern Sierra Nevada forest soils collected near fossil leaf localities have extremely low abundances of soil tetraether compounds and are not a likely contaminant source for ancient materials.

Leaf-Margin Temperature Estimates: In order to assess the accuracy of GDGT temperatures across the ancient Sierra landscape, we calculated the mean-annual temperature at three, previously described fossil leaf localities by comparing the proportion of whole-margined to toothed leaves. The binomial uncertainty associated with this approach ranges from 2-4 degrees due to the relatively small number of leaves included in these estimates (Table S2). In all cases, paleobotanical temperature estimates overlap with GDGT temperature data. Sea-level MBT/CBT temperatures are further supported by recent temperature estimates (21±4) from lateritic goethites in associated paleochannel sediments (Yapp, 2008). Thus, it seems clear that GDGT temperature data record realistic temperature changes across the paleo-landscape. However, in some cases, GDGT temperatures are slightly warmer than paleobotanical values. While uncertainty in the GDGT calibration could be the cause of the temperature discrepancy, it is not surprising that

paleobotanical methods produce lower temperature estimates along the altitudinal gradient: 1) riparian environments have higher proportion of non-entire species than adjacent forest making it likely that fluvial settings produce underestimates of MAT (Kowalski and Dilcher, 2003); 2) there can be a possible taphonomic bias against preservation of some types of leaves (Greenwood et al., 2004); 3) the relationship between soil and mean annual temperatures may differ depending on the depth of microbial GDGT production; and 4) examination of GDGT temperatures from a modern elevation transect shows some MBT/CBT temperatures up to several degrees warmer than mean annual temperatures.

Modern Sierra Nevada Temperatures: Modern climatic data for California and the Sierra Nevada mountains were compiled from National Oceanographic and Atmospheric Association Data for comparison with ancient MBT/CBT data. MAT in the modern N. Sierra decreases from ~17°C at elevations <50 m to ~3°C at elevations greater than 2500 m (Fig. DR2) by 5.5°C/km (R^2 = 0.91; n = 56 stations). MAT reconstructions at fossil floral localities were determined using the regression line for data from latitude 39-40°N and longitude -122 to -120°W, a range overlapping our sample sites.

Thermodynamic Model for ΔT and $\Delta\delta D$ with Elevation: To couple paleotemperature and paleoelevation data, we used a model for the isotopic evolution of precipitation during orographic lifting of an airmass that incorporates moist static energy, water vapor content, and condensate isotope composition along ascending airmass trajectories (Rowley et al., 2001). This model utilizes initial conditions of temperature and relative humidity and calculates the cooling of the airmass along the dry adiabat until saturation occurs, after which the airmass is subject to progressive rainout and wet adiabatic cooling. The thermodynamically controlled adiabatic lapse is dependent upon the starting T and RH once saturation is achieved. We utilized this empirical model to calculate the weighted mean elevation for a measured $\Delta\delta^{18}O$ using a range of starting

temperature and RH conditions. ΔδD is then calculated from model outputs for $\Delta\delta^{18}O$ elevation relationships and the assumption of meteoric composition, which is demonstrated in altitudinal gradients in high temperature, high humidity tropical environments (Gonfiantini et al., 2001). Uncertainties in this approach are determined by the frequency distribution of $\Delta\delta_{precip}$ versus elevation and is reported as 2σ, based on model outputs (Rowley, 2007). Modeled Eocene temperature lapses with elevation are 5.3°C/km for elevations of 0-3 km and calculated $\Delta\delta D_{precip}$ for elevations 0-3000 m is ~1.4‰/100 m. This lapse rate is smaller than the modern and that used in prior paleoelevation reconstructions of the Eocene Sierra Nevada (Mulch et al., 2006), due primarily to differences in starting sea-level temperature (Rowley, 2007). Uncertainties in reconstructed paleoelevations reported using $\Delta\delta D_{nC31}$ and ΔT_{GDGT} reflect the uncertainties associated with model output results for starting T and RH conditions (Rowley, 2007).

Sea-level δD_{nC31} is used to calculate $\Delta\delta D_{nC31}$ along the paleo-channels. This is calculated using a linear regression of stream-channel distances against δD_{nC31}. The intercept of the data at 0 km distance gives a value of -168‰, a value identical to the heaviest measured value near the Eocene shoreline. Paleoelevation is calculated from the $\Delta\delta D_{nC31}$ using relative sea-level δD_{C31}= -168‰ and a polynomical fit to $\Delta\delta D_{precip}$ versus elevation relationship (Fig. DR4).

Recent estimates of sea-level δD_{precip} from Eocene Sierra Nevada laterites (-61‰) are significantly more D-depleted than that produced by Mulch et al. 2006 (-43‰) and values for modern precipitation. Calculated ε values for Eocene angiosperms are consistent with estimated sea-level δD_{precip} of Mulch et al. (2006) however they are not incompatible with more recent estimates. D-depleted Eocene sea-level precipitation would produce smaller apparent fractionations between leaf-waxes and precipitation than has been observed, however our assumption of constant ε across the paleorange results in no change in reconstructed paleoelevations.

Paleoelevations calculated from ΔT use a starting sea-level temperature of 24.5°C. This base temperature fits model results for ΔT and $\Delta\delta D_{nC31}$ due to orographic lifting and rainout. Lower sea-level temperature inputs produce lower paleoelevation estimates for temperature and isotope-based data. However, model inputs of sea-level temperatures <24.5°C produce negative elevations at near-shoreline sites and require δD_{nC31} at sea-level to be more negative to fit model results and measured data. Moreover, low sea-level temperatures are incompatible with isotopic data, which provide a degree of constraint on starting model temperature inputs. Paleoelevation estimates from modeled temperature and isotope lapse rates in general within 100 m and 200 m of estimates produced using constant lapse rates of 1.4‰/100m and 5.3°C/km.

Comparison of Paleoelevation Estimates: Fossil leaf localities cover a broader latitudinal range than Eocene kaolinites from the paleo-Yuba river. Reconstructed paleoelevation estimates from organic molecular proxies are equal to or higher than authigenic mineral estimates (Fig. DR5) with respect to distance along the upstream channel relative to the Eocene ocean margin. Both datasets show steep river gradients.

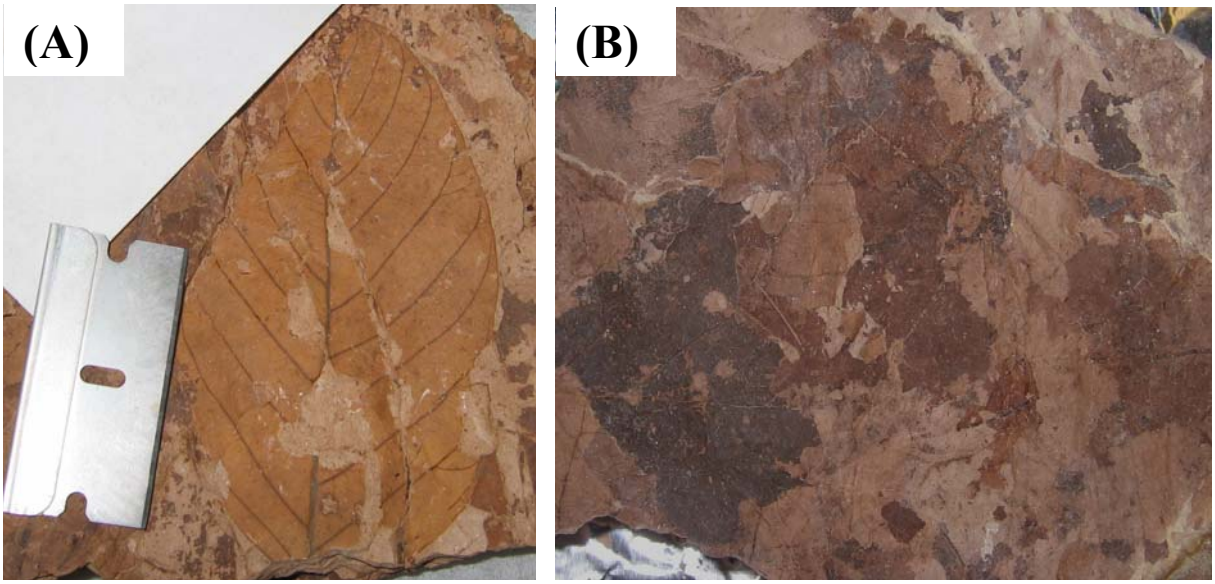

Figure DR1. (A) Individual fossil leaf (*Rhamnidium Chaneyii)* from the Buckeye paleofloral locality. Individual leaves retain original leaf-cuticle and are identified by paleobotanical methods. (B) Bulk leaf-mat at the Sailor Flats locality. Fossil leaves and leaf cuticle are preserved from a variety of plant types in overbank and floodplain sediments.

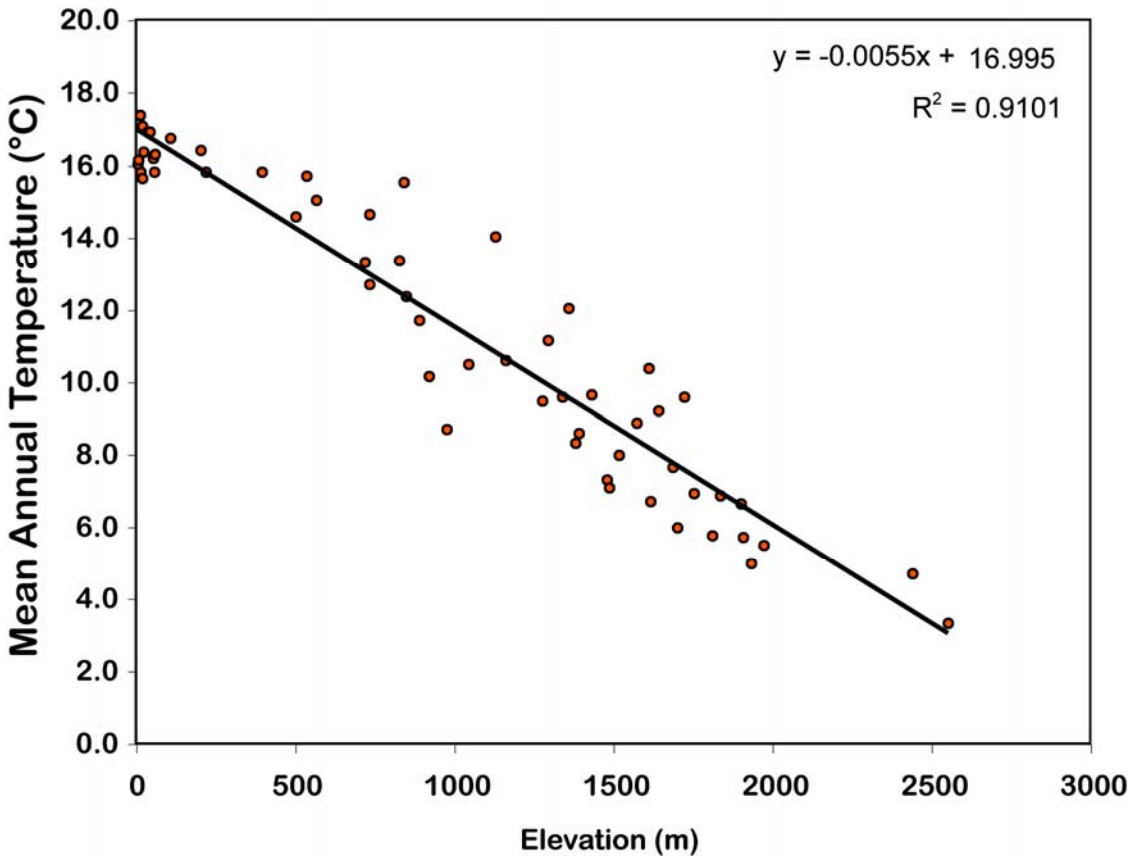

Figure DR2. Modern mean annual temperature data as a function of elevation at long-term California climate stations between 39-40°N latitude and 120-122°W longitude. Paleofloral localities are not directly associated with modern climate stations. The relationship between MAT (°C) and elevation is used to calculate modern MAT at fossil leaf localities for comparison of ancient and modern temperatures.

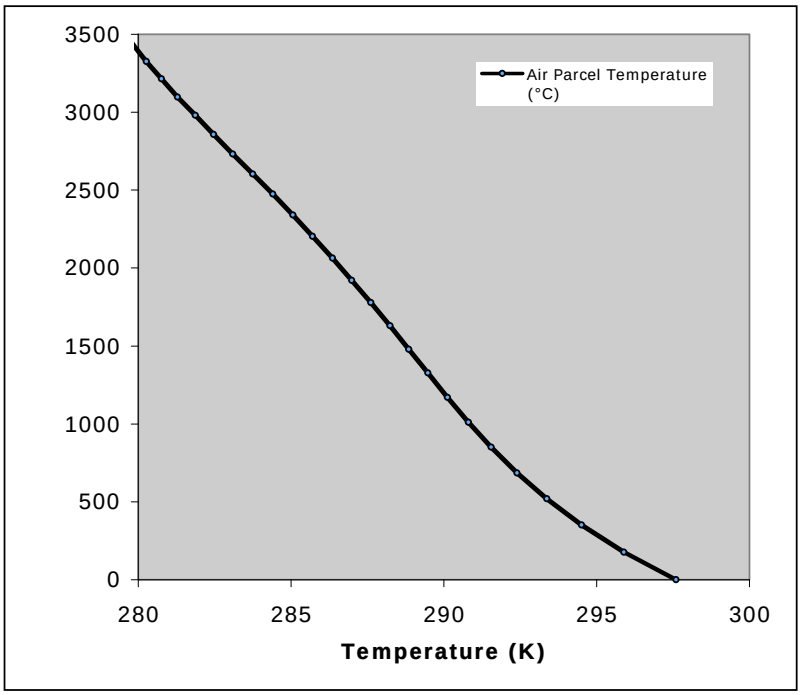

Figure DR3. Polynomial fit to the output of a thermodynamic model that calculates the change in temperature associated with condensation of precipitation from an airmass during orographic ascent for initial conditions of 24.5°C and 82% relative humidity. The predicted $\Delta T_{airmass}$ as a function of elevation is empirically calibrated using modern data from low to mid-latitudes (Rowley et al., 2001). We assume $\Delta T_{airmass}$ with elevation is a reasonable fit for ΔT_{MAT} with elevation. Based on starting conditions, the predicted temperature lapse of 5.3°C/km for elevations 0-3000 m is slightly lower than the modern global average temperature lapse but consistent with measured temperature lapse along a modern humid, tropical altitudinal gradient (Gonfiantini et al., 2001). Lower lapse rates produce higher paleoelevation estimates for a given ΔT. A polynomial fit to the model results is used to calculate paleoelevation from organic molecular proxy data.

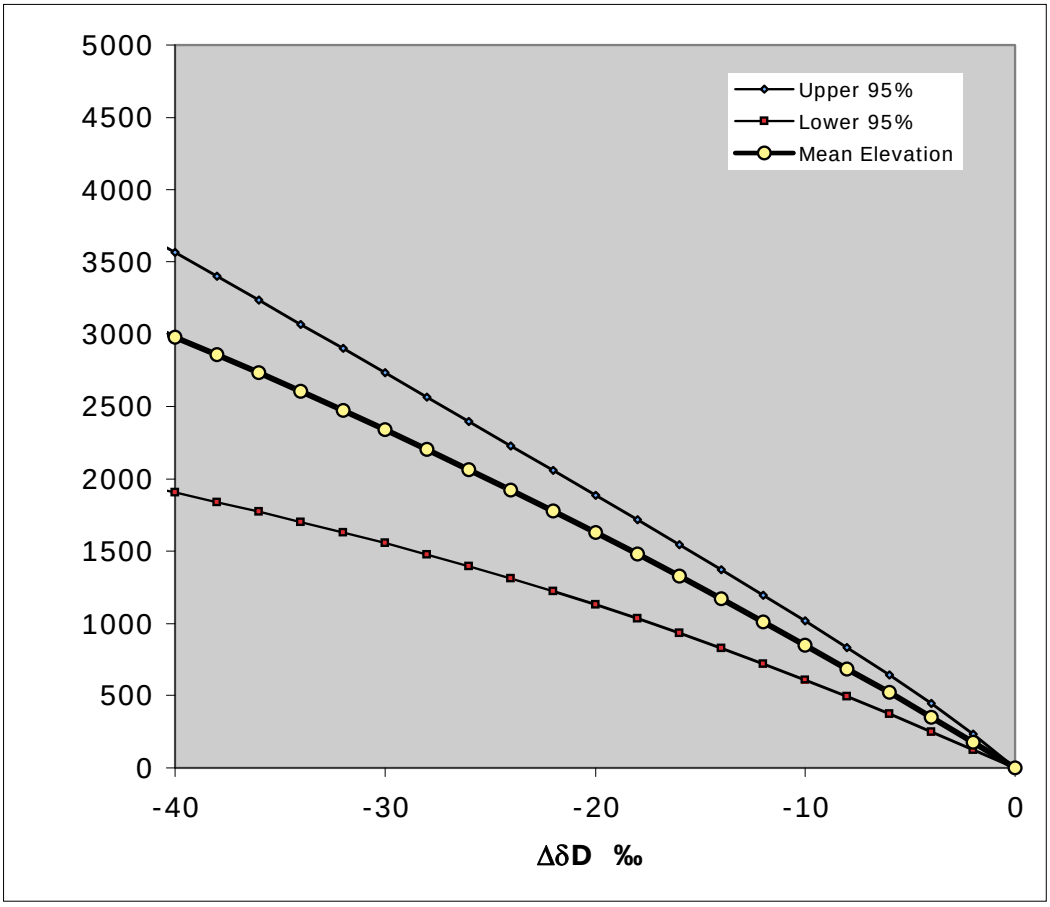

Figure DR4. Output of a thermodynamic model that calculates the mean elevation as a function of the measured $\Delta\delta D_{precip}$ for initial conditions of 24.5°C and 82% relative humidity. Model output for mean elevation is based on $\Delta\delta^{18}O$, but converted to $\Delta\delta D$ by assuming the precipitation falls along a Meteoric Water Line (slope 8). The predicted mean elevation for a measured $\Delta\delta D_{precip}$ is empirically calibrated using modern data from low to mid-latitudes. Model uncertainty is based on the 2σ uncertainty resulting from the probability density distribution of corresponding starting T and RH. The relationship between $\Delta\delta D$ and elevation for elevations of 1000 to 2000 m (1.4‰/100 m) is slightly lower than modern due to the higher temperature constraints for early Eocene sample sites. Colder temperatures produce lower weighted elevations as a function of $\Delta\delta D_{precip}$. A polynomial fit to the model results is used to calculate paleoelevation from organic molecular proxy data

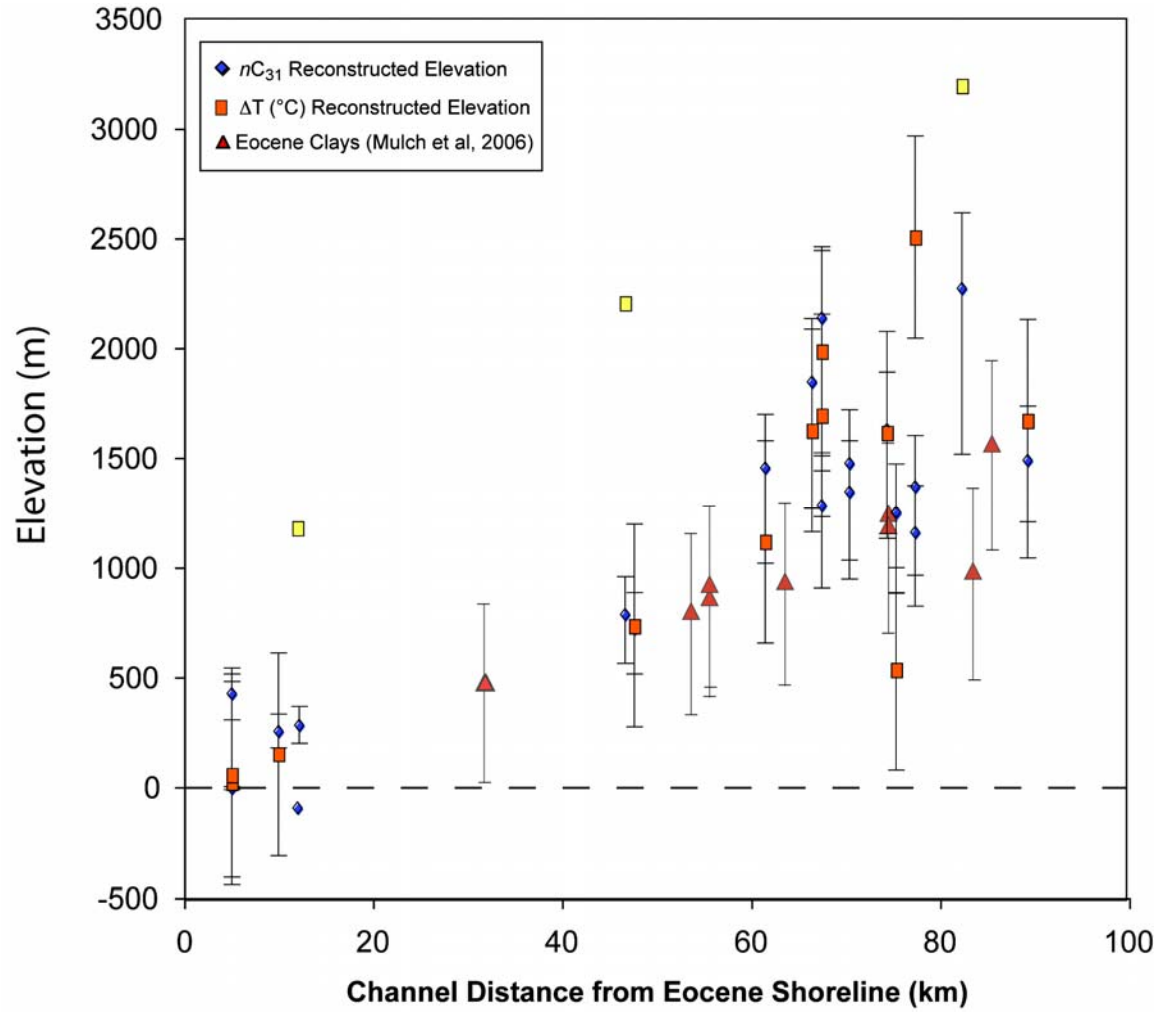

Figure DR5. Reconstructed paleoelevations from MBT/CBT temperatures, $\Delta\delta D_{nC31}$, and $\Delta\delta D_{kaolinite}$. Three independent proxies show high elevations along the length of the Sierra Nevada paleo-channels. Organic molecular proxies produce slightly higher paleoelevation estimates than $\Delta\delta D_{kaolinite}$ (Mulch et al., 2006) due to higher temperature (~2.5°C) inputs for the thermodynamic model. Yellow squares reflect paleoelevation estimates from sites with T_{GDGT} consistent with downstream transport of organic compounds.

Table 1. Fossil Leaf Localities

Locality	Latitude	Longitude	Modern Elev. (m)	Channel Distance [1]	Distance Along Line A-A'	*n*-Alkane δD 25	27	29	31	33	Eocene Elevation (C_{31})[2]	(+/-)[3]	Eocene Elevation (ΔT)[4]	(+/-)[5]	Eocene Temperature[6]	CPI
China Gulch	38.260	-120.889	162	5	5	-193	-191	-175	-168	-170	1	7/5	29	460	24.5	4.1
Camanche Bridg	38.259	-120.892	162	5	5	-193	-188	-178	-173	-176	435	107/121	63	460	23.7	0.0
Pentz	39.650	-121.564	220	10	9	-160	-171	-179	-171	-	264	73/74	158	460	22.6	4.1
Cherokee Site 1	39.635	-121.543	347	12	9	-168	-176	-177	-167	-168	-88	-	1186	460	17.1	5.6
Cherokee Site 2	39.635	-121.543	347	12	9	-172	-176	-168	-171	-167	291	79/82	-	460		5.4
Fiona Hill	39.103	-120.853	811	47	30	-177	-168	-182	-177	-164	792	162/223	2207	460	12.5	5.1
Council Hill	39.593	-120.994	1321	68	47	-169	-182	-185	-184	-173	1288	218/379	1697	460	14.8	5.3
Iowa Hill	39.113	-120.853	841	48	31	-175	-180	-184	-177	-170	728	153/204	742	460	19.1	5.1
Stewart Mine	39.163	-120.848	878	78	35	-179	-182	-182	-182	-188	1165	205/339	-	460		4.4
You Bet 2	39.213	-120.884	884	75	34	-191	-193	-192	-188	-180	1634	259/500	1619	460	15.1	4.6
Chalk Bluffs - E	39.207	-120.880	933	76	34	-177	-180	-187	-183	-168	1255	215/368	544	460	20.1	5.1
Chalk Bluffs - W	39.207	-120.880	933	76	34	-184	-183	-187	-183	-190	1256	215/369	-	460		4.5
Scotts Flat	39.271	-120.913	945	67	35	-198	-197	-193	-191	-185	1850	290/582	1629	460	15.1	4.6
Gold Bug	39.372	-120.924	957	62	40	-184	-186	-189	-186	-175	1461	238/438	1123	460	17.3	4.6
Hidden Gold Can	39.162	-120.856	969	78	34	-183	-192	-189	-185	-180	1373	228/408	2507	460	11.1	5.1
Buckeye Flat - E	39.246	-120.888	975	71	36	-180	-179	-185	-184	-176	1350	225/400	-	460		5.8
Buckeye Flat - W	39.246	-120.888	975	71	36	-183	-180	-182	-186	-184	1479	240/445	-	460		5.6
Woolsey Flat	39.415	-120.863	1183	68	47	-196	-196	-196	-195	-	2141	341/698	1988	460	13.5	2.7
Mountain Boy	39.655	-120.951	1463	83	54	-179	-207	-204	-197	-200	2272	369/754	3195	460	7.8	3.8
Pine Grove 1	39.720	-120.896	1652	90	62	-187	-186	-185	-186	-186	1494	245/450	1674	460	14.9	6.0

[1]Distance from Eocene ocean shoreline (Ione Fm) after Mulch et al. 2006

[2]Based on modeled Eocene isotopic lapse curve from Rowley for 24.5□C sea-level T and RH = 81.5

[3]Error includes error (2 σ) from isotopic lapse with elevation and estimated δD composition at sea level.

[4]Based on modeled Eocene temperature lapse curve from Rowley for 24.5□C sea-level T and RH = 81.5

[5]Error based on 2 σ error in fit of modern temperature/elevation relationship.

[6]Eocene mean annual surface temperature from GDGT soil temperature proxy

Table 2. Leaf-margin temperature estimates

Locality	Channel Distance	Distance A-A'	Toothed	Entire	Total	P	MAT[1]	Error (□C)
Iowa Hill	48	31	14	13	27	0.48	15.3	3.2
Buckeye Flat	71	36	25	23	47	0.48	15.2	2.7
Chalk Bluffs	76	34	28	30	58	0.52	16.3	2.5

[1] Based on regression of Miller et al. 2006

References

Barthlott, W., and Neinhuis, C., 1997, Purity of the sacred lotus, or escape from contamination in biological surfaces: Planta, v. 202, p. 1–8.

Climatography of the United States No. 81. Monthly Station Normals of Temperature, Precipitation, and Heating and Cooling Degree Days 1971-2000.

Cranwell, P.A., Eglington G., and Robinson N., 1987, Lipids of aquatic organisms as potential contributors to lacustrine sediments. 2: Organic Geochemistry, v. 11, p. 513-527.

Eglington, G. and Hamilton, R.J., 1967, Leaf epicuticular waxes: Science, v. 156, p. 1322-1334.

Flanagan, L.B., Comstock, J.P., and Ehleringer, J.R., 1991, Comparison of modeled and observed environmental influences on the stable oxygen and hydrogen isotope composition of leaf water in *Phaseolus vulgaris L.*: Plant Physiology, v. 96, p. 588-596.

Gonfiantini, R., Roche, M., Olivry, J.C., Fontes, J.C., and Zuppi, G.M., 2001, The altitude effect on the isotopic composition of tropical rains: Chemical Geology, v. 181, p. 147-167.

Greenwood D. R. P. Wilf S. L. Wing D. C. Christopher, 2004, Paleotemperature estimation using leaf-margin analysis: is Australia different?: Palaios, v. 19, p. 129-142.

Holloway, P. J., 1969, The effects of superficial wax on leaf wettability: Annals of Applied Biology, v. 63, p.145-153.

Huguet, C., 2007, TEX86 paleothermometry: proxy validation and application in marine sediments. [PhD Thesis] Utrecht University.

Kowalski E. A. and Dilcher, D. L., 2003, Warmer paleotemperatures for terrestrial ecosystems: Proceedings National Academy Sciences, v. 100, p. 167-170.

Schimmelman A., Lewan, M.D., and Wintsch, R.P., 1999, D/H isotope ratios of kerogen, bitumen, oil, and water in hydrous pyrolysis of source rocks containing kerogen types I, II, IIS, and III: Geochimica et Cosmochimica Acta, v. 63, p. 3751-3766.

Schouten, S., Hopmans, E.C., Pancost, R.D. and Sinninghe Damsté, J.S., Widespread occurrence of structurally diverse tetraether membrane lipids: evidence for the ubiquitous presence of low-temperature relatives of hyperthermophiles: Proceedings of the National Academy of Sciences, v. 97, 14421–14426.

Schouten, S., E. Hopmans, A. Forster, Y. van Breugel, M. M. M. Kuypers, and J. S. Sinninghe Damsté, 2003, Extremely high sea-surface temperatures at low latitudes during the middle Cretaceous as revealed by archaeal membrane lipids: Geology v., 31, p. 1069-1072.

Schouten, S., E.C. Hopmans, and J.S. Sinninghe Damsté, 2004, The effect of maturity and depositional redox conditions on archaeal tetraether lipid palaeothermometry: Organic Geochemistry, v. 35, p. 567-571.

Sinninghe Damsté, J.S., Hopmans, E.C., Pancost, R.D., Schouten, S. and Geenevasen, J.A.J., 2000, Newly discovered non-isoprenoid dialkyl diglycerol tetraether lipids in sediments: Chemical Communications p. 1683–1684.

Sinninghe Damsté, J.S., Ossebaar, J., Schouten, S., and Verchuren, D., 2008, Altitudinal shifts in the branched tetraether lipid distribution in soil from Mt. Kilimanjaro (Tanzania): Implications for the MBT/CBT continental paleothermometer, Organic Geochemistry, v. 39, 1072-1076.

Sluijs A., Schouten S., Pagani M., Woltering M., Brinkhuis H., Damste´ J. S. S., Dickens G. R., Huber M., Reichart G. J., Stein R., Matthiessen J., Lourens L. J., Pedentchouk N., Backman J., and Moran K., 2006, Subtropical arctic ocean temperatures during the Palaeocene/Eocene thermal maximum: Nature, v. 441, p. 610–613.

Squires, R.L., 1997, Taxonomy and distribution of the Buccinid gastropod Brachysphingus for the uppermost Cretaceous and lower Cenozoic marine strata of the Pacific slope of North America: Journal of Paleontology, v. 71, p. 847–861.

van de Vossenberg, J. L. C. M., A. J. M. Driessen, and W. N. Konings, 2000, Adaptations of the cell membrane for life in extreme environments. In Cell and Molecular Response to Stress Vol. 1: Environmental Stressors and Gene Responses: *in* K. B., Storey and J.M. Storey (eds.), Elsevier.

Weijers, J. W. H., Schefuß, E., Schouten, S. and Sinninghe Damsté, J. S., 2007c, Coupled thermal and hydrological evolution of tropical Africa over the last deglaciation: Science, v. 315, p. 1701-1704.

Yang H., and Huang Y.S., 2003, Preservation of lipid hydrogen isotope ratios in Miocene lacustrine sediments and plant fossils at Clarkia, Northern Idaho, USA: Organic Geochemistry, v. 34, p. 13-423.